Electromagnetic Scattering From Multiple Single-Walled Carbon Nanotubes Having Tumbleweed Configurations

Ahmed M. Hassan, *Member, IEEE*, Fernando Vargas-Lara, Jack F. Douglas, and Edward J. Garboczi

***Abstract*— Carbon nanotubes (CNTs) exhibit highly complicated structures when incorporated in composites and are neither perfectly straight nor aligned in any one direction. Recently, the "clumpy" structure of multiple aggregated CNTs has been likened to desert tumbleweeds. The goal of this paper is to quantify the electromagnetic scattering characteristics of CNTs in the tumbleweed configuration using classical electromagnetic simulations. The simulation results show that the first-plasmon resonance, exhibited by an individual CNT, splits into multiple resonances when multiple CNTs agglomerate into tumbleweed configurations. The number of the resonances increases linearly with the number of CNTs inside the tumbleweed. The second-plasmon resonance exhibits similar splitting behavior. This splitting in the plasmon resonances is caused by the asymmetry of shapes of CNTs and their proximity to each other. If sufficient CNTs agglomerate, the split first-plasmon and second-plasmon resonances overlap, leading to an overall broadband behavior. These results indicate the importance of precise modeling of CNT shapes and the distribution of shapes on the electromagnetic response. Our computations qualitatively explain the broadband response of CNT films and composites and should aid in the development of novel broadband materials and devices based on CNTs.**

***Index Terms*— Carbon nanotubes (CNTs), composites, conductivity, electromagnetic scattering, plasmon resonances.**

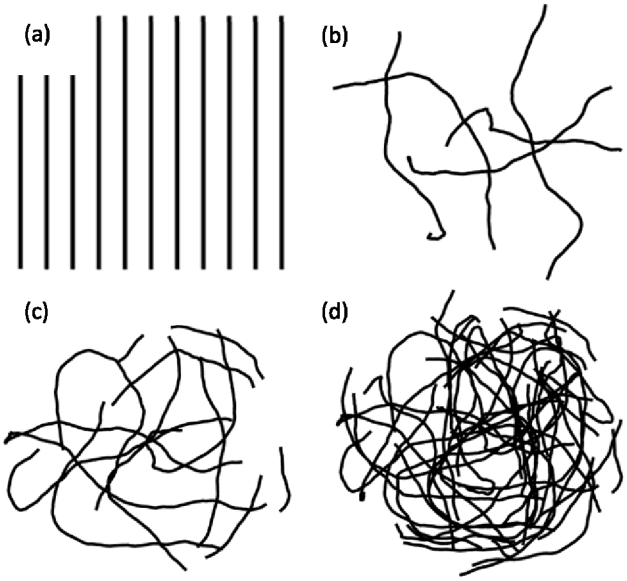

Fig. 1. Schematic illustration of representative CNT domains having multiple CNT in (a) uniform, straight, aligned configuration, (b) tumbleweed configuration with 5 CNTs, (c) tumbleweed configuration with 10 CNTs, and (d) tumbleweed configuration with 32 CNTs.

I. Introduction

COMMERCIAL forms of carbon nanotubes (CNTs) normally exhibit structures more complex than the term tube would imply [1]–[7]. Instead, CNTs typically take the form of bushy domains that resemble desert tumbleweeds [1], [2]. The study of CNT tumbleweeds is receiving increasing interest because of the desire to realistically model these complex additives to determine how their structure and dispersion influence the mechanical, thermal, and electrical properties of CNT/polymer composites [1]–[7]. In particular, the full-wave electromagnetic scattering response from CNT tumbleweeds is expected to be greatly influenced by the shape of these complex-shaped nanoparticles. An understanding of the electromagnetic response of CNTs is essential in the development of techniques that use microwave and terahertz radiation for the nondestructive evaluation of CNT composites being developed for the aerospace industry [8]. Our work also suggests that the unique electromagnetic response of CNT tumbleweeds might be utilized in the development of novel broadband devices and absorbers. These unique electromagnetic effects derive from highly shape-dependent optical resonances whose frequencies directly reflect the shape heterogeneity of the CNT tumbleweeds; we thus focus computationally on this aspect of the electromagnetic response of these nanoparticles.

While the electromagnetic characteristics of straight and aligned CNTs, similar to those shown in Fig. 1(a), have been

Manuscript received November 23, 2016; revised March 15, 2017; accepted March 29, 2017. Date of publication April 5, 2017; date of current version May 31, 2017. This work was supported by the National Institute of Standards and Technology (NIST) through the project "Carbon Nanocomposite Manufacturing: Processing, Properties, Performance." The work of A. M. Hassan was supported in part by the NIST under Award 70NANB15H285 and in part by the NSF CRI under Award 1629908. The work of F. Vargas-Lara was supported by the NIST under Award 70NANB13H202 and Award 70NANB15H282. *(Corresponding author: Ahmed M. Hassan.)*

A. M. Hassan is with the Computer Science and Electrical Engineering Department, University of Missouri-Kansas City, Kansas City, MO 64110 USA(e-mail: hassanam@umkc.edu).

F. Vargas-Lara and J. F. Douglas are with the Material Measurement Laboratory, Materials Science and Engineering Division, National Institute of Standards and Technology, Gaithersburg, MD 20899 USA (e-mail: luis.vargaslara@nist.gov; jack.douglas@nist.gov).

E. J. Garboczi is with the Material Measurement Laboratory, Applied Chemicals and Materials Division, National Institute of Standards and Technology, Boulder, CO 80305 USA (e-mail: edward.garboczi@nist.gov).

Color versions of one or more of the figures in this paper are available online at http://ieeexplore.ieee.org.

Digital Object Identifier 10.1109/TAP.2017.2691475

given extensive attention [9]–[17], there has been essentially no previous systematic study of the full-wave electromagnetic response of CNTs having the common tumbleweed morphology [see Fig. 1(b)–(d)] normally encountered in commercial CNT composites. Recently, we developed techniques to study the static and the dynamic electromagnetic response of individual metallic single-walled CNTs with realistic shapes [16], [17]. In our previous studies, we showed that worm-like CNTs exhibited first-plasmon and second-plasmon resonances whereas perfectly straight CNTs only exhibited first-plasmon resonances in their extinction cross-section spectrum [17]. In this paper, we extend this past analysis to study, for the first time, the resonance effects in multiple CNTs having tumbleweed configurations. In particular, when multiple CNTs are grouped into a tumbleweed configuration, we show that the first plasmon and second plasmon split into additional resonances whose number increase with the number of CNTs per tumbleweed. Our findings reveal that the electromagnetic scattering characteristics of CNT domains depend strongly on the number of CNTs that form the domain, the CNT individual shapes, and the CNTs position within the domain. Therefore, the present study highlights the importance of taking into consideration the shapes and distributions of CNTs in order to accurately study their electromagnetic scattering characteristics.

This paper is arranged as follows. In Section II, we describe the geometrical properties of the tumbleweed CNT configurations and how their electromagnetic response was calculated. Section III shows the numerical results and Section IV discusses the applications of these results. Finally, the conclusions and future work are presented in Section V.

II. Methods

A. CNT Tumbleweed Model

It is extremely challenging to simulate accurately all the forces that act on CNTs and lead to their agglomeration into the tumbleweed form. Therefore, we developed a coarse-grained molecular dynamics (CGMD) model that generated random CNT shapes that structurally resemble the tumbleweeds in commercial composites [6], [16], [17]. Examples of the tumbleweed configurations generated by the model are presented in Fig. 1(b)–(d). Fig. 1(b)–(d) shows tumbleweeds with $N = 5$, $N = 10$, and $N = 32$ CNTs, respectively. These numerically generated tumbleweeds resemble the distribution of CNTs in commercial tumbleweeds [1]–[7].

The details of this CGMD are contained in previous publications [6], [16], [17]. Briefly, in our CGMD model each CNT is modeled as a string of beads where adjacent connected beads interact via a tunable potential that modulates the persistence length of each CNT [6], [16], [17]. The persistence length is a measure of straightness. Lower persistence lengths correspond to highly twisted CNTs and higher persistence lengths correspond to straighter CNTs [6], [16], [17]. A persistence length of 83 nm was assumed for all the CNTs in this paper [17]. In this CNT coarse—grained representation, each bead corresponds to several carbon atoms, since modeling each carbon atom in the CNT is computationally expensive. The CNT configurations were obtained by solving the Newton's equations of motion of this CNTs coarse-grained model via molecular dynamics simulations [6], [16], [17]. A CNT domain, referred here as CNT tumbleweed, is created by forcing interacting CNTs to stay within a spherical shell of diameter 130 nm [6], [16], [17]. In all the tumbleweeds, the CNTs are assumed to be single-walled and metallic with (9, 9) chirality, radius $a = 0.61$ nm, and contour length $L_{\mathrm{CNT}} = 96$ nm. Commercial metallic single-walled CNTs and reference CNT materials have lengths distributions that vary from 50 to 4000 nm [18], [19]. The longer the CNT, the larger the computational time required to simulate its electromagnetic response. Since the main goal of this paper is to study the interactions between multiple CNTs, we selected relatively short CNTs with $L_{\mathrm{CNT}} = 96$ nm to allow the simulation of a large number of CNTs, N, in a feasible computational time. The (9, 9) chirality and the radius $a = 0.61$ nm were chosen as a representative example. The distributed impedance and the polarizability of individual metallic single-walled CNTs is weakly dependent on the radius [20]. Therefore, metallic CNTs with different radii and chiralities, will yield similar results to those reported in this paper using (9, 9) CNTs [17]. All the CNTs had identical Drude-like surface conductivity with a relaxation time of $\tau = 3$ ps and a static, dc conductivity $\sigma_0 = 0.235$ S as follows [17]:

$$\sigma = \frac{\sigma_0}{1 + j\omega\tau}. \tag{1}$$

The conductivity, σ, in (1) has both a real and imaginary part. The real part controls the peak amplitude and the bandwidth of the CNTs resonances [17]. The imaginary part of the conductivity in (1) controls the frequency of the resonance and induces the CNTs to resonate at a frequency that is much lower than the frequency of perfectly conducting wires with the same shape and size [9]–[17]. Therefore, CNTs of length L achieve a first resonance at a frequency that ranges between $0.01c_0/2L$ and $0.02c_0/2L$ where c_0 is the speed of light in vacuum [17]. A perfectly conducting wire of the same size and shape will achieve a first resonance at $c_0/2L$. Therefore, CNTs exhibit a first resonance at a wavelength that is 50–100 times larger than the size of the CNT [9]–[17].

Tumbleweeds containing $N = 2, 5, 10, 20$, and 32 non-branching worm-like CNTs per tumbleweeds were generated. At least $M = 70$ different configurations, for each value of N, were generated for this tumbleweeds, using the CGMD model. The only parameter that was varied between tumbleweed configurations was the shape of the CNTs within the tumbleweed and the internal arrangement of the CNTs in the tumbleweed. All other factors such as the length, conductivity, and the persistence length of the CNTs, were kept the same. In a realistic tumbleweed, these factors also vary, but the goal of this paper is to highlight the importance of CNT agglomeration on the electromagnetic scattering characteristics. Real tumbleweeds are apparently branched structures rather than simply aggregates of worm-like CNTs, but exact information about the topology is currently unknown. In all our tumbleweed models, the CNTs were constrained to not self-intersect. Even though there is extensive literature on the dc/static electric properties

of intersecting CNTs [21], [22] to the best of our knowledge, there is very little work reporting the dynamic electromagnetic properties of intersecting CNTs in the microwave and terahertz range. If these data become available, they can easily be incorporated into the numerical method used in this paper. Moreover, the static values for the contact resistance, due to tunneling of electrons between two intersecting CNTs, indicate a large dc contact resistance, and therefore our assumption that the CNTs are not intersecting is adequate as a first order approximation [21], [22]. It is important to emphasize that all the geometrical and conductivity values chosen in this paper serve as examples to illustrate the concept. Assigning different values will affect the locations of the resonances and their spectral width, but the major findings of this paper will still hold.

B. Method of Moments Formulation for Arbitrary Thin Wires

In this paper, we used an in-house-developed method of moments (MoMs) formulation for arbitrary thin wires (ATWs) to calculate the full-wave classical electromagnetic response of the tumbleweeds due to a linearly polarized incident plane wave [17], [23]. In this formulation, each CNT is approximated as equivalent 1-D wire with an impedance equivalent to that of the 3-D structures. This approximation leads to no detectable loss in accuracy, since CNTs exhibit large aspect ratios, with their contour lengths significantly larger than their diameters. Therefore, from an electromagnetic point of view they can be simulated as 1-D wires with a high reduction in computational cost and without any loss in accuracy [17]. This reduction in computational time is essential for the simulation of the hundreds of tumbleweed configurations, containing thousands of CNT, studied in this paper. This large number of configurations is necessary to accurately quantify the effect of the shape of the tumbleweeds.

Even though the MoM for ATW is computationally more efficient than the 3-D simulation, the computational complexity associated with simulating a tumbleweed with a large number of CNTs is still significant. We start by noting that each CNT was discretized into 100 pixels to accurately capture its shape. This corresponds to 98 current basis functions per CNT [23]. Therefore, 3136 current basis functions or unknowns were solved for at each frequency for an $N = 32$ tumbleweed. The computational time for an $N = 32$ tumbleweed was 1.5 hours per frequency on an Intel[1] Xeon Processor E5-2687W with 20M Cache and 3.10-GHz processor base frequency. We calculated the tumbleweed response at 301 frequencies between 15 and 45 THz to capture the sharp resonances typically exhibited by CNTs. Therefore, each $N = 32$ tumbleweed required ~450 computational hours to calculate its full response. Since each frequency is independent, the MoM for ATW code was parallelized to run on 20 cores and therefore the calculation of the response of a single $N = 32$ tumbleweed required approximately 24 h. As we noted in the prior section, at least $M = 70$ different configurations were tested for each N value. Due to this computational cost, we only considered a range of $N = 2$ to $N = 32$ CNTs per tumbleweed. This range of N provided a wide enough range to clarify the trend in the plasmonic resonances of CNT tumbleweeds and we considered a maximum of $N = 32$ to keep the computational complexity at a feasible level.

The primary electromagnetic scattering parameter calculated is the total extinction cross section, C_{ext}, which is defined as the sum of the total scattering cross section C_{scat} and the total absorption cross section C_{abs} from each tumbleweed. In this paper, we will focus on the frequency range near the first and second-plasmon resonances, which is in the low-frequency range with respect to the CNT size. For nanoparticles in the low-frequency range, C_{abs} is typically much larger than C_{scat} [24]. Therefore, $C_{\text{ext}} \approx C_{\text{abs}}$ and in all the following results the extinction cross section, C_{ext}, and the absorption cross section C_{abs} can be used interchangeably.

In this paper, we will focus on the frequency range from 15 to 45 THz to cover the first-plasmon and the second-plasmon resonances of the CNTs [17]. At the first-plasmon resonance, the CNT axial current is approximately a single lobe sinusoid, i.e., maximum near the center of the CNT and minimum at its ends. The charge distribution on a CNT resembles a dipole at the first-plasmon resonance being maximum at the CNT's ends with one end being positive and the other being negative [25]. Therefore, the first-plasmon resonance is typically labeled as a dipolar resonance. At the second-plasmon resonance, the axial current is sinusoidal with a double lobe whereas the charge distribution resembles that of a quadrupole exhibiting maxima at the ends and a maximum near the center of each CNT with an opposite polarity. Therefore, the second-plasmon resonance is typically depicted as a quadrupolar resonance [25]. Resonances with similar current and charge distributions have been reported in many nanostructures and microstructures using slightly different labels [26].

III. Numerical Results

A. Dimer and Trimer ($N = 2$ and $N = 3$) Tumbleweeds

The simplest model tumbleweed is a dimer, which consists of $N = 2$ CNTs, as shown in Fig. 2(a). In this tumbleweed, both CNTs are nonstraight and nonintersecting. Moreover, Fig. 2(a) shows three views of the 3-D $N = 2$ tumbleweed to clarify the complexity of the 3-D shapes of the CNTs. In each view, the direction of the incident wave and electric field is shown. These directions were arbitrary chosen and do not affect the main conclusions in Fig. 2 due to the randomness in the shapes of the CNTs in the tumbleweed. When each CNT is simulated separately, each CNT exhibits a resonance at approximately 22 THz in its extinction cross section spectrum as shown in Fig. 2(b). The resonance of a single CNT was found to be mainly dependent on CNT conductivity and contour length and only weakly dependent on shape [17]. Therefore, the reason that the two CNTs in Fig. 2(a) resonate at approximately the same frequency, when they are simulated individually, is that they have the same length and conductivity.

[1]Certain commercial equipment, instruments, or materials are identified in this paper to foster understanding. Such identification does not imply recommendation or endorsement by the National Institute of Standards and Technology, nor does it imply that the materials or equipment identified are necessarily the best available for the purpose.

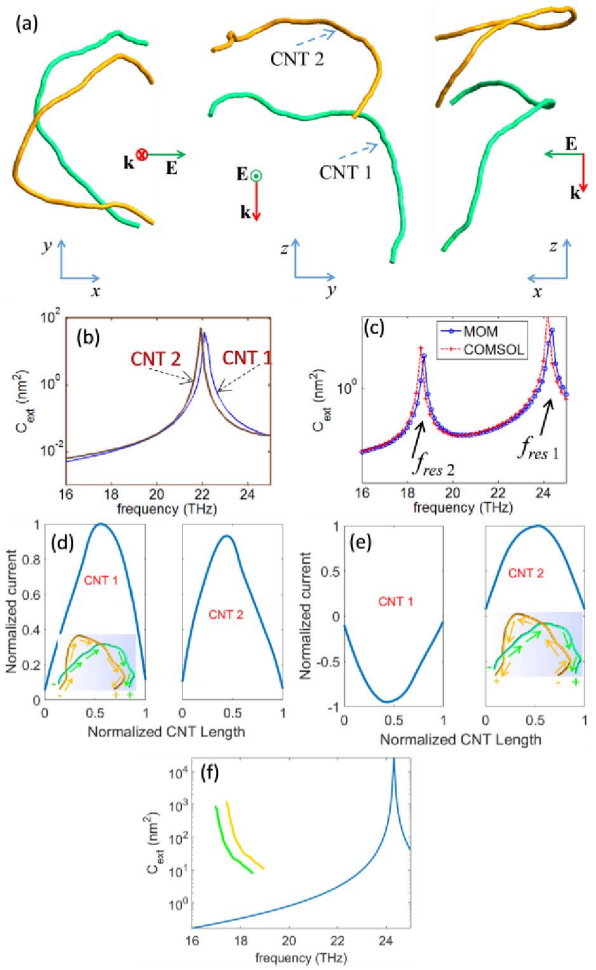

Fig. 2. (a) Rendering of a representative configuration of a tumbleweed formed by two nonintersecting CNTs. Three different views are shown to clarify the 3-D complexity of the tumbleweed. In each view, **k** vector indicates the direction of the incident wave, and **E** vector indicates the direction of the electric field. (b) Extinction cross section from each CNT in the tumbleweed by itself. (c) Extinction cross section from the tumbleweed. (d) Axial current distribution on the CNTs at the bonding resonance f_{res1}. (e) Axial current distribution on the CNTs at the antibonding resonance f_{res2}. (f) Extinction cross section from a tumbleweed with two CNTs with identical shapes.

Fig. 2(c) shows the extinction cross section of the two CNTs in the tumbleweed configuration, shown in Fig. 2(a), calculated using our in house developed MoMs formulation for ATWs and the independent 3-D commercial finite-element package COMSOL. The close agreement between the two curves in Fig. 2(c) validates our implementation of the MoM formulation for ATW. There are two resonances in Fig. 2(c), f_{res1} at a higher frequency than the resonance of the individual CNTs, which we will term the bonding mode, and f_{res2} at a lower frequency, which we will term the antibonding mode. Therefore, the resonance of an isolated CNTs splits into two resonances when placed in a dimer configuration. This splitting has been previously reported for a plethora of asymmetric nano-dimers [27]–[29]. However, in the majority of previously reported cases of resonance splitting, the bonding and the antibonding resonances were created by choosing two noble metal nanoparticles of the same shapes and different sizes [27], two equal nanoparticles with different orientation [27], two nanoparticles of different materials [28], or two nanoparticles with different canonical shapes like a nano-cube/nano-sphere dimer [29]. We likewise observe a mode splitting for CNT dimers with complex nonuniform shapes, as illustrated in Fig. 2(a).

To understand the physical basis of this mode splitting, we plotted the instantaneous axial current of the CNTs at the bonding mode in Fig. 2(d) and at the antibonding mode in Fig. 2(e). Typical of resonances at the first-plasmon resonance, the current on each CNT resembles a single lobe sinusoidal where the current is maximum at approximately the middle of the CNT and drops to zero at its ends [17]. The charges on the CNTs are minima at the center of each CNT and are maxima in magnitude at the ends, with one end positive and the other end negative. At the bonding resonance, the currents on both CNTs are in phase pointing in the same direction. The charges are also in phase meaning that adjacent ends hold charges with the same polarity. Regarding the antibonding mode, the CNT currents still resemble a single lobe sinusoidal, but they are antiphase being positive on one CNT and negative on the other. Adjacent CNT ends also hold opposite charges as shown in Fig. 2(e). Therefore, the first-plasmon resonance of individual CNTs splits, in general, into two resonances when placed in a dimer configuration.

It is important to emphasize that if a different incident wave direction or if a different electric field polarization is exerted, the peak amplitude of the resonances will change since the coupling between the incident wave and the tumbleweed will change. However, two resonances will still be observed, similar to Fig. 2(c), as long as there is nonsymmetry in the CNT shapes. If the two CNTs in Fig. 2(a) have the same shape, the antibonding resonance would disappear as shown in Fig. 2(f) when a different CNT dimer, composed of two slightly displaced CNTs with the same shape, is simulated. In the case of the symmetrical dimer, the antibonding resonance vanishes because the symmetric out of phase currents completely cancel in the scattered fields.

As noted before, a similar behavior has been demonstrated in numerous gold and silver nano-dimers [27]–[29]. If two symmetric nanoparticles are simulated, only a single resonance is exhibited. If nonsymmetry is introduced, the resonance splits into two resonances and the charge distribution at each resonance is similar to that in Fig. 2(d) and (e). Fig. 2 reports this mode splitting for the first time for CNTs. Moreover, the high aspect ratio of CNTs provides a wider possible variability in CNT shape that cannot be achieved with gold nanoparticles with lower aspect ratios [27], and this large aspect ratio leads to a greater separation between the bonding and antibonding modes. The dimer case is presented herein only as a prelude to the tumbleweed cases with $N > 2$ CNTs, which is the main focus of this paper.

A tumbleweed with three CNTs is shown in Fig. 3(a). Again all the CNTs in this tumbleweed have the same length and complex conductivity, but each CNT has a different shape. In this case, the first-plasmon resonance splits into three resonances as shown in Fig. 3(b). Fig. 4(a)–(c) shows the CNT axial currents at these three first-plasmon resonances for the $N = 3$ tumbleweed in Fig. 3(a). Fig. 4(a)–(c) confirms

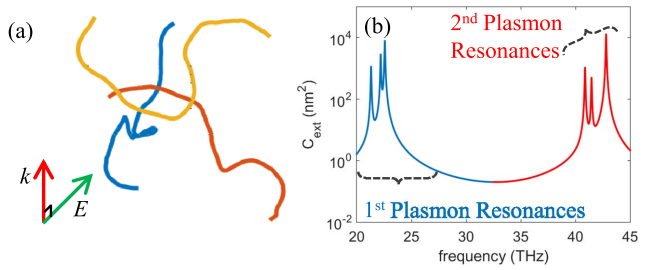

Fig. 3. (a) Schematic of one tumbleweed configuration having three nonintersecting CNTs. The directions of the incident wave k, and electric field E are indicated. (b) Extinction cross section from the tumbleweed.

that these resonances are of the first-plasmon resonance type because the axial current on each CNT is approximately sinusoidal with only one main lobe at the center [17].

Mode splitting having similar features has also been exhibited in gold nano-trimers [30]–[32]. In this case, a quasi-electrostatic approximation, where the nanoparticles were modeled as dipoles, was used to calculate the split in the resonances. The interactions between the dipoles were then represented by a 3×3 coupling matrix [30], [31]. In the gold nano-trimer system, the condition for the resonance was achieved when the real part of the determinant of the coupling matrix was equal to zero. For trimers of asymmetric gold nanoparticles, there are in general three possible solutions that will satisfy this condition, which justifies the splitting of the first-plasmon resonance into three resonances [30], [31]. However, the coupling matrix formulation is based on the electrostatic dipole approximation that is valid: 1) when the incident wavelength is much larger than the nanoparticle and 2) the field is uniform throughout each nanoparticle. For the CNT tumbleweed trimer in Fig. 3, the wavelength is ≈ 50 times larger than the CNTs [17]. However, because of the complicated shapes of the CNTs, the field cannot be assumed uniform throughout each CNT. For example, if the incident electric field is in the x-direction, some of the CNT segments in the tumbleweed in Fig. 3(a) will be tangential to the x-axis and the incident electric field, and some of the CNT segments will be normal to the electric field. Therefore, full-wave electromagnetic solvers, such as the MoM for ATW, are needed to accurately calculate the splitting of the first-plasmon resonance into three resonances as in the case of the tumbleweed with $N = 3$ CNTs shown in Fig. 3(a).

One of the main contributions of this paper is to investigate the second-plasmon resonance when three CNTs are grouped into a tumbleweed configuration. As shown in red in Fig. 3(b), the second-plasmon resonance was also found to split into three separate resonances for a nonsymmetric trimer. If each CNT in the tumbleweed in Fig. 3(a) is simulated by itself they will all show a second-plasmon resonance at approximately the same frequency, as reported in [17], which indicates that the splitting of the second-plasmon resonance is due to the interactions between the CNTs in the trimer tumbleweed configuration. The reason that we classify these three resonances as a second-plasmon resonance is the fact that the current on each CNT exhibits a second-plasmon behavior with a double lobe sinusoidal current as shown in Fig. 4(d)–(f). The results in Figs. 3 and 4 indicate that for a trimer of asymmetric nanoparticles, not only the first-plasmon resonance splits into three distinct resonances, but higher order modes such as the second-plasmon resonances also exhibit the same splitting behavior.

B. Tumbleweeds With $N > 3$ CNTs

In this section, we expand the number of CNTs per tumbleweed to $N = 5, 10, 20$, and 32. In all the cases, the CNTs had the same contour length, persistence length, and complex axial conductivity. Therefore, for each N, only the shapes and locations of the CNTs were varied. This is the first time that such a large number of nanostructures, per domain, with such a large variation in shape, have been studied.

Fig. 5(a)–(c) shows the extinction cross section of three tumbleweeds with $N = 5$, $N = 10$, and $N = 32$ CNTs, respectively. The curve is divided into two parts, with the low frequencies shown in blue and the high frequencies shown in red, in order to visually clarify the first-plasmon and the second-plasmon resonances, respectively. The resonances were classified as first-plasmon or second-plasmon resonances by investigating the axial currents carried by the CNTs. Similar to Fig. 4(a)–(c), if the currents on the majority of the CNTs had a single sinusoidal lobe, the resonance was classified as a first-plasmon resonance whereas if the majority of the CNTs had a current with a double sinusoidal lobe, similar to Fig. 4(d)–(f), the resonance was classified as a second-plasmon resonance. For the case of $N = 5$ in Fig. 5(a), it is clear that the first-plasmon resonance of an individual CNT splits into five distinct resonances, shown in blue, and the second-plasmon resonance also splits into five distinct resonances, shown in red. For other tumbleweeds, the number of resonances increases linearly with N as indicated in Fig. 5(b) and (c). However, as the number of resonances increase, they start to overlap, and therefore they become harder to resolve, as shown in Fig. 5(b) and (c).

As N increases, the first-plasmon and second-plasmon resonances start to spread over a wider bandwidth, and the separation between the first-plasmon and the second-plasmon resonances starts to decrease as shown by the progression from Fig. 5(a)–(c). To clarify this decrease in separation, $M = 70$ different tumbleweed configurations were simulated for each of the following numbers of CNTs per tumbleweed ($N = 1, 5, 10, 20, 32$). For each N, the average frequency difference, Δf, between the first-plasmon resonance with the highest frequency and the second-plasmon resonance with the lowest frequency, was calculated and plotted in Fig. 5(d). It is clear that this frequency difference, Δf, decreases as the number of CNTs per tumbleweed, N, increases. Since typical real tumbleweeds contain hundreds of CNTs, the difference Δf is expected to vanish, judging by the extrapolation of Fig. 5(d) for N much larger than 32. Therefore, the results in Fig. 5 predict that, for tumbleweeds with a large number of CNTs, the split first-plasmon and second-plasmon resonances are anticipated to overlap leading to a wide or broadband frequency response. To clarify this broadband response, Fig. 6(a) and (b) shows the extinction cross section from all

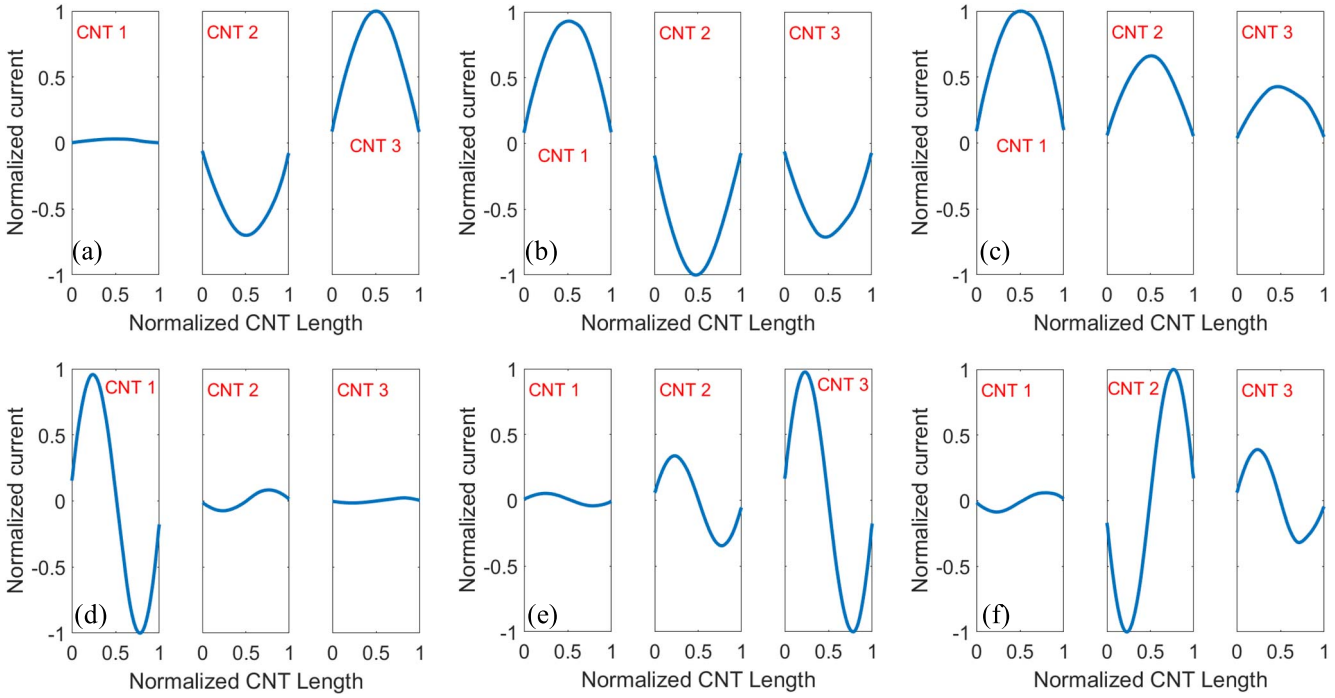

Fig. 4. CNTs' axial currents for the $N = 3$ tumbleweed in Fig. 3 at the (a) first, (b) second, and (c) third first-plasmon resonance. The CNTs' axial currents at the (d) first, (e) second, and (f) third second-plasmon resonance.

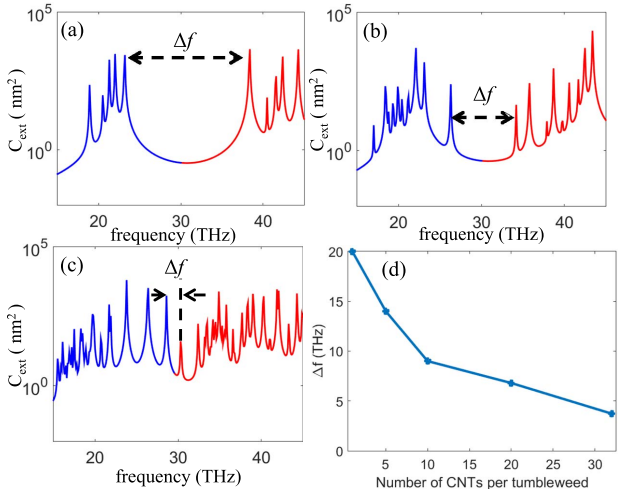

Fig. 5. Extinction cross section of a single tumbleweed with (a) $N = 5$ CNTs, (b) $N = 10$, (c) $N = 32$ CNTs/tumbleweed, and (d) average frequency difference between the first-plasmon resonance with the highest frequency and the second-plasmon resonance with the lowest frequency.

$M = 70$ different tumbleweeds with $N = 5$ and $N = 32$ CNTs/tumbleweed, respectively. The first-plasmon resonances are shown in blue, and the second-plasmon resonances are shown in red. For the case of $N = 5$ in Fig. 6(a), the first-plasmon resonances covered a frequency range varying from ≈18 to ≈24 THz whereas the second-plasmon resonances covered a frequency range varying from ≈33 to ≈45 THz. For the case of $N = 32$ in Fig. 6(b), it can be seen that the resonances of the 70 tumbleweeds covered the whole band from 15 to 45 THz, and it was hard to separate the first-plasmon and the second-plasmon resonances.

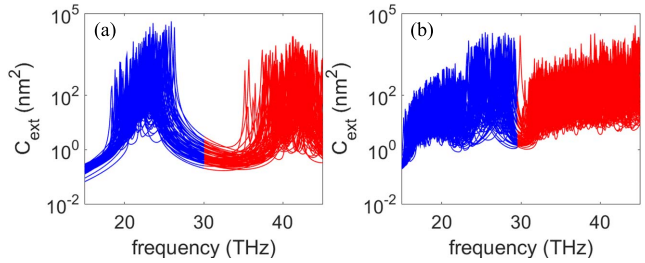

Fig. 6. Extinction cross section of $M = 70$ different tumbleweeds with (a) $N = 5$ CNTs and (b) $N = 32$ CNTs.

We can gain some insight into the physical impact of these resonances by calculating the effective dielectric permittivity of a composite containing 70 different randomly oriented tumbleweeds in the dilute limit. The main assumption in the dilute limit is that the tumbleweeds are far enough apart so that the electromagnetic coupling between different tumbleweeds can be neglected. To quantify the minimum separation between two tumbleweeds, so that the tumbleweed–tumbleweed coupling can be neglected, we simulated two CNT tumbleweeds with various separations as shown in Fig. 7. Each of the two tumbleweeds in Fig. 7, one shown in blue and the other in red, had $N = 5$ CNTs, and special care was taken to maintain the condition that none of the tumbleweeds intersected at any separation. Fig. 7(a)–(c) shows the extinction cross section when the center-to-center distance between the tumbleweeds was 13, 33, and 130 nm, respectively. In each of these three figures, we also show the extinction cross section of each tumbleweed when simulated in isolation. In Fig. 7(a), when the two tumbleweeds are closest, it is clear that the extinction cross section of the two tumbleweeds is significantly different

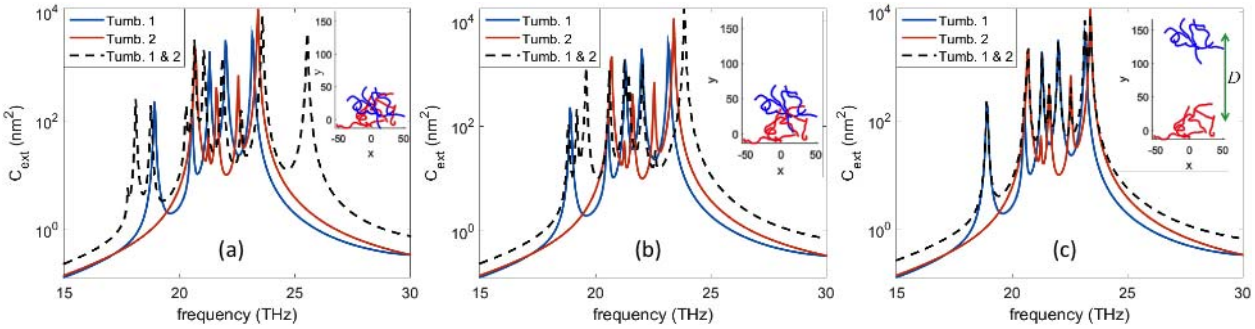

Fig. 7. Extinction cross section of two nonintersecting tumbleweeds each with $N = 5$ CNTs separated by a center-to-center distance (D) (a) $D = 13$ nm, (b) $D = 33$ nm, and (c) $D = 130$ nm.

from that of each tumbleweed in isolation. Therefore, at the center-to-center separation in Fig. 7(a), there is still strong electromagnetic interaction between the two tumbleweeds causing the resonances to shift and hybridize. As the center-to-center separation between the tumbleweeds, D, increases, the resonances of the two tumbleweeds become simply a superposition of the resonances of each tumbleweed by itself as shown in Fig. 7(c). Fig. 7 then demonstrates that if $D \geq 130$ nm, which corresponds to the constructed diameter of each tumbleweed, the coupling between the tumbleweeds can be neglected. This is in accordance with the values reported in other nanostructures where the shifts in resonances were found to rapidly diminish when the separation between the nanostructures exceeded the particle size [33], [34].

Based on the previous analysis, the dilute limit approximation of the effective dielectric permittivity of a composite of CNT tumbleweeds is valid when the separation between the tumbleweeds exceeds their average size. However, within a tumbleweed, the dilute limit is not valid, so that the electromagnetic properties of a tumbleweed are not simply the sum of the individual CNT properties, as was also shown above. Therefore, the first step in calculating the effective dielectric permittivity of a composite containing multiple CNT tumbleweeds is to replace each tumbleweed with an induced electric, $\mathbf{p}$, and magnetic, $\mathbf{m}$, dipole moment. These dipole moments are related to the local electric field, $\mathbf{E}$, and the local magnetic field, $\mathbf{H}$, at the tumbleweed by the following relation [26], [35]–[39]:

$$\begin{bmatrix} \mathbf{p} \\ \mathbf{m} \end{bmatrix} = \begin{bmatrix} \boldsymbol{\alpha}_{\mathbf{ee}} & \boldsymbol{\alpha}_{\mathbf{em}} \\ \boldsymbol{\alpha}_{\mathbf{me}} & \boldsymbol{\alpha}_{\mathbf{mm}} \end{bmatrix} \begin{bmatrix} \mathbf{E} \\ \mathbf{H} \end{bmatrix} \tag{2}$$

where $\boldsymbol{\alpha}_{\mathbf{ee}}$, $\boldsymbol{\alpha}_{\mathbf{em}}$, $\boldsymbol{\alpha}_{\mathbf{me}}$, and $\boldsymbol{\alpha}_{\mathbf{mm}}$ are the electric–electric, electric–magnetic, magnetic–electric, and magnetic–magnetic polarizability tensors, respectively [26], [35]–[39]. However, the CNTs in the tumbleweeds resonate at frequencies that are much lower than the resonance frequencies of perfectly conducting wires of identical size and shape. CNTs resonate at such lower frequencies due to the imaginary part of the conductivity in (1). Therefore, in the range of frequencies considered in this paper, we are operating in the low-frequency regime where $\boldsymbol{\alpha}_{\mathbf{ee}}$ is much larger than the $\boldsymbol{\alpha}_{\mathbf{em}}$, $\boldsymbol{\alpha}_{\mathbf{me}}$, and $\boldsymbol{\alpha}_{\mathbf{mm}}$ and, therefore, it will dominate the effective dielectric permittivity of the composite [35]–[36]. Therefore, in this paper we will focus only on the calculation of $\boldsymbol{\alpha}_{\mathbf{ee}}$ which we will designate as $\boldsymbol{\alpha}$ for conciseness.

The dynamic polarizability tensor $\boldsymbol{\alpha}^i$ for tumbleweed i can be calculated as [40]

$$\boldsymbol{\alpha}^i = -\frac{j}{\omega\varepsilon_0} \sum_{n=1}^{N} \int \mathbf{J}_n(\ell) \partial \ell \tag{3}$$

where $\mathbf{J}_n(\ell)$ is the axial current flowing on CNT n in tumbleweed i, calculated using the full-wave MoM for ATW formulation, and the summation is performed over all the CNTs in the tumbleweed. Equation (3) summarizes the nine components, of which six are independent, of the symmetric polarizability tensor $\boldsymbol{\alpha}^i$. For example, to calculate the α^i_{xy} component, the incident electric field is set in the x-direction and the y-component of the axial current $\mathbf{J}_n(\ell)$ is selected in the integration in (3) [40]. Once the polarizability tensor is calculated, its diagonal components are used to calculate the average intrinsic conductivity $[\sigma^i]$ per CNT in tumbleweed i as follows [41], [42]:

$$[\sigma^i] = \frac{1}{3}\left(\alpha^i_{xx} + \alpha^i_{yy} + \alpha^i_{zz}\right) / V_{\mathrm{CNT}} \tag{4}$$

where V_{CNT} is the volume of the N CNTs in tumbleweed i defined as $V_{\mathrm{CNT}} = N(\pi a^2 L_{\mathrm{CNT}})$ where a is the radius of each CNT and L_{CNT} is the contour length of each CNT. We emphasize that (4) gives the average intrinsic conductivity of a single CNT inside a tumbleweed, since the parameter V_{CNT} contains a factor of N in the denominator. If a composite is made up of M randomly oriented tumbleweeds, we repeat the calculation of (4) for each tumbleweed and then perform a second average, with respect to the different tumbleweeds, to calculate the effective "intrinsic conductivity"

$$[\sigma(N)] = \frac{1}{M} \sum_{i=1}^{M} [\sigma^i] \tag{5}$$

where the N in $[\sigma\ (N)]$ refers to the number of CNTs within each tumbleweed. In (5), we selected $M = 70$ as a number large enough to lead to a convergent $[\sigma\ (N)]$. Note that $[\sigma(N)]$ in (5) is the average intrinsic conductivity of a CNT inside a tumbleweed, averaged over both the internal structure of the tumbleweed and averaged over M different realizations of the N-CNT tumbleweed. Using (5) we calculated the effective intrinsic conductivity $[\sigma(5)]$ and $[\sigma(32)]$ for tumbleweeds with

$N = 5$ CNTs and $N = 32$ CNTs, respectively. Following (5), the relative effective permittivity of a tumbleweed composite can be expressed as [41], [42]:

$$\varepsilon^{\text{eff}} = \varepsilon_r^{\text{eff}} - j\varepsilon_i^{\text{eff}} = \varepsilon_h\left(1 + \phi_{\text{total}}[\sigma(N)] + O\left(\phi_{\text{total}}^2\right)\right) \quad (6)$$

where ε_h is the permittivity of the host medium and ϕ_{total} is the total volume fraction of CNTs in the composite. We can use a dilute limit approximation as shown in (6) since the intrinsic conductivity was properly computed for the nondilute CNTs within the tumbleweeds. We used a total volume fraction $\phi_{\text{total}} = 0.025$ % for both the $N = 5$ and $N = 32$ cases, where ϕ_{total} is the total volume fraction of CNTs in the composite, not the volume fraction of tumbleweeds approximated as roughly 130-nm-diameter particles. Given the geometrical information above about the CNTs, it is easily seen that the volume fraction of CNTs within a nominal 130-nm-diameter tumbleweed sphere is about 0.05% for $N = 5$ and 0.32% for $N = 32$. Suppose one were to pack these tumbleweed spheres in a face-centered-cubic arrangement in a composite structure, so that the center–center distance was 130 nm, which was shown above to be large enough to justify the noninteracting tumbleweed approximation and hence the dilute limit approximation. The volume fraction of CNTs in the composite would then be about $0.74 \times 0.05\%$ for $N = 5$ or 0.037%, and $0.74 \times 0.32\%$ for $N = 32$, or about 0.24% [43], [44]. Therefore, the volume fraction of 0.025%, for both the tumbleweeds with $N = 5$ and $N = 32$ CNTs, is low enough to justify the dilute limit approximation in (6).

It is important to emphasize that our work is different from previous reports where the CNTs are considered to be uniformly dispersed and the distance between any CNT pair is large enough to justify the dilute limit approximation. In the uniformly dispersed case, we can still use (6) and the same total volume fraction but with the intrinsic conductivity of a single CNT [45]. However, in this paper, the CNTs are in close proximity within each tumbleweed and they are strongly coupled and, therefore, the full-wave calculation of the tumbleweed's dynamic polarizability and intrinsic conductivity is needed as defined in (3) and (4). After calculating the polarizability and intrinsic conductivity of the tumbleweed using (3) and (4), we can now accurately use (6), provided that the spacing between the tumbleweeds in the composite is large enough to justify the dilute limit approximation, which is satisfied in our case. For simplicity, in (6) the host medium is assumed to take its free space permittivity value, $\varepsilon_h = 1$.

Fig. 8(a) and (b) shows a sketch of a tumbleweed composite with $N = 5$ CNTs/tumbleweed and $N = 32$ CNTs/tumbleweed, respectively. The sketches in Fig. 8(a) and (b) are not to scale, but they present an illustration of how the tumbleweeds are packed inside the composites represented by (3)–(6). The circles in Fig. 8(a) and (b) represent the extents of the tumbleweed. Therefore, there are only two media in Fig. 8(a) and (b): 1) the host medium with dielectric permittivity ε_h and 2) the CNTs. To have the same total volume fraction in both composites, the number of tumbleweeds in Fig. 8(b) is approximately one-sixth of the tumbleweeds in Fig. 8(a) since the tumbleweeds in Fig. 8(b) have approximately six times the number of CNTs than those in Fig. 8(a).

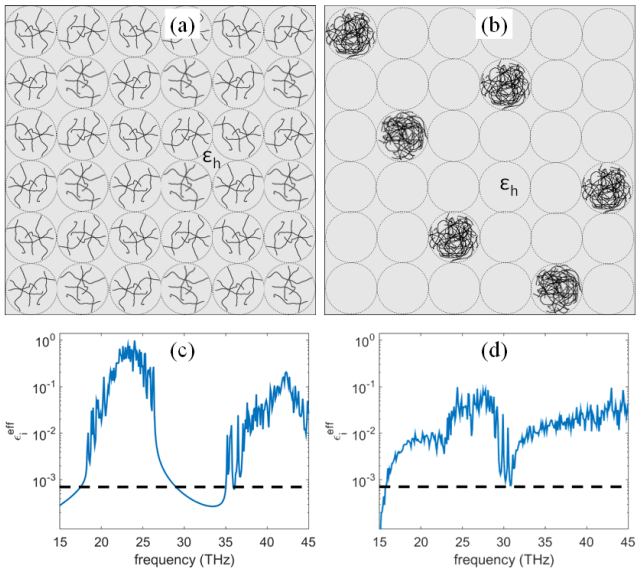

Fig. 8. (a) Sketch of a tumbleweed composite each with $N = 5$ CNTs/tumbleweed. (b) Sketch of a tumbleweed composite each with $N = 32$ CNTs/tumbleweed. (c) Imaginary part of the effective relative dielectric permittivity of a composite composed of tumbleweeds with (c) $N = 5$ CNTs/tumbleweed and (d) $N = 32$ CNTs/tumbleweed. The actual CNT volume fraction in both composites was 0.025%.

Fig. 8(c) and (d) shows the imaginary component of the effective dielectric permittivity, $\varepsilon_i^{\text{eff}}$ for this simple composite, made from $N = 5$ in Fig. 8(a) and $N = 32$ CNT tumbleweeds in Fig. 8(b), respectively. In Fig. 8(c), for $N = 5$, the contribution to $\varepsilon_i^{\text{eff}}$ due to the first-plasmon resonances and the contribution to $\varepsilon_i^{\text{eff}}$ due to the second-plasmon resonances are well separated. If we take an arbitrary value as our cutoff, for example $\varepsilon_i^{\text{eff}} \geq 7 \times 10^{-4}$, the bandwidth for $N = 5$ in Fig. 8(c) is two well-separated frequency ranges 17.5 THz $\leq f \leq$ 28.9 THz and 35 THz $\leq f$. Using the same cutoff, the bandwidth for the $N = 32$ case in Fig. 8(d) is a single broadband defined as $f \geq 15.8$ THz. Therefore, by comparing Fig. 8(c) and (d) it is clear that, as the number of CNTs per tumbleweed increases, the bandwidth of the effective permittivity for a simple composite evolves from two separate frequency ranges into one overlapping broadband frequency range. This increase in bandwidth cannot be obtained with perfectly aligned straight CNTs and is a direct consequence of the randomness of the shapes and orientation of the CNTs within the tumbleweeds.

IV. Discussion

The results in this paper show that the randomness in the shape and orientation of CNTs in tumbleweeds has a strong effect on their electromagnetic scattering characteristics. This randomness in shape and orientation led to the splitting of the first-plasmon and the second-plasmon resonances into new resonances whose number increased with the number of CNTs per tumbleweed. The splitting of the resonances also led to a continuous decrease in the separation between the first-plasmon and the second-plasmon resonances. These results were achieved using tumbleweeds with up to $N = 32$ CNTs per tumbleweed. Since this splitting of resonances was

achieved consistently for all values of N considered in this paper we predict that practical tumbleweeds with hundreds of CNTs per tumbleweed will exhibit a similar behavior. Moreover, the electrostatic properties of tumbleweeds were previously demonstrated to exhibit a steady behavior for tumbleweeds with a few CNTs per tumbleweed all the way to tumbleweeds with 250 CNTs per tumbleweed [6]. Similarly, we predict that the resonance splitting in the dynamic response of tumbleweeds, demonstrated in this paper for up to $N = 32$ CNTs per tumbleweed, will continue to hold for practical tumbleweeds with a larger number of CNTs.

These results will also open up several new research areas. For example, several experimental measurements have demonstrated broadband absorption peaks in the response of metallic nanotube and nanowire films/composites [46]–[49]. The exact shape of these nanotubes and nanowires was not considered in these studies. This paper shows that the variations in the shape and the orientation of these nanotubes might be responsible, at least in part, for the broadband peaks recorded in measurements on commercial CNT materials.

Another research area that these results open up is the use of variations in shape to create novel broadband materials and devices. Varying the size has been utilized for a long time to develop broadband and multiband antennas [50], [51]. This paper shows that variations in shape, especially in high aspect ratio nanotubes and nanowires, can generate similar effects. Shape variation provides an additional degree of freedom that can be used to tune the total number of resonances, their exact location, the level of overlap between the first-plasmon and second-plasmon resonances, and the overall bandwidth of the tumbleweeds. This mode splitting and the consequent broadband response are not unique to CNTs, but it can also be exhibited in other nanowires that have tumbleweed-like structures, and could even be scaled to the microwave range using centimeter-length perfectly conducting wires. For other wires, whose resonance frequencies are more comparable to their lengths, substantial $\alpha_{\mathbf{em}}$, $\alpha_{\mathbf{me}}$, and $\alpha_{\mathbf{mm}}$ in (2) can be achieved in these tumbleweed structures leading to unique electric and magnetic properties which will be the focus of our future work.

V. Conclusion

The extinction cross sections of hundreds of tumbleweeds, with varying number of CNTs per tumbleweed, have been calculated using the MoMs for ATWs formulation. The results show that, in comparison to isolated CNTs, the resonances in the extinction cross sections of tumbleweeds with multiple CNTs split into additional resonances whose number increase linearly with the number of CNTs per tumbleweed. This resonance splitting was demonstrated for both the first-plasmon and the second-plasmon resonances and is attributed to the discrepancy in the shapes and orientations of the CNTs within a tumbleweed. Moreover, as the number of CNTs per tumbleweed increases, the first-plasmon and second-plasmon resonances were found to spread over a wider bandwidth and eventually overlap, leading to an overall broadband response. The effective dielectric permittivities of dilute tumbleweed composites were also calculated, and they also demonstrate a corresponding broadband response. These results demonstrate, for the first time, the importance of complex tumbleweed shapes in explaining the electromagnetic measurements of nanotube and nanowire composites, and they can be used, in the future work, as the basis for developing novel devices and materials.

References

[1] A. W. K. Ma, M. R. Mackley, and S. S. Rahatekar, "Experimental observation on the flow-induced assembly of Carbon nanotube suspensions to form helical bands," *Rheol. Acta*, vol. 46, no. 7, pp. 979–987, Aug. 2007.

[2] A. W. K. Ma, M. R. Mackley, and F. Chinesta, "The microstructure and rheology of carbon nanotube suspensions," *Int. J. Mater. Forming*, vol. 1, no. 2, pp. 75–81, Jul. 2008.

[3] S. R. Vora, B. Bognet, H. S. Patanwala, F. Chinesta, and A. W. K. Ma, "Surface pressure and microstructure of carbon nanotubes at an air-water interface," *Langmuir*, vol. 31, no. 16, pp. 4663–4672, Apr. 2015.

[4] J. M. Brown *et al.*, "Hierarchical morphology of carbon single-walled nanotubes during sonication in an aliphatic diamine," *Polymer*, vol. 46, no. 24, pp. 10854–10865, Nov. 2005.

[5] G. Faiella, F. Piscitelli, M. Lavorgna, V. Antonucci, and M. Giordano, "Tuning the insulator to conductor transition in a multiwalled carbon nanotubes/epoxy composite at substatistical percolation threshold," *Appl. Phys. Lett.*, vol. 95, no. 15, p. 153106, 2009.

[6] F. Vargas-Lara and J. F. Douglas, "Confronting the complexity of CNT materials," *Soft Matter*, vol. 11, no. 24, pp. 4888–4898, 2015.

[7] R. M. Mutiso and K. I. Winey, "Electrical properties of polymer nanocomposites containing rod-like nanofillers," *Prog. Polym. Sci.*, vol. 40, pp. 63–84, Jan. 2015.

[8] C. S. Davis *et al.*, "Cure temperature influences composite electrical properties by carbon nanotube-rich domain formation," *Compos. Sci. Technol.*, vol. 133, pp. 23–32, Sep. 2016.

[9] G. Miano and F. Villone, "An integral formulation for the electrodynamics of metallic carbon nanotubes based on a fluid model," *IEEE Trans. Antennas Propag.*, vol. 54, no. 10, pp. 2713–2724, Oct. 2006.

[10] G. W. Hanson, "Fundamental transmitting properties of carbon nanotube antennas," *IEEE Trans. Antennas Propag.*, vol. 53, no. 11, pp. 3426–3435, Nov. 2005.

[11] P. J. Burke, S. Li, and Z. Yu, "Quantitative theory of nanowire and nanotube antenna performance," *IEEE Trans. Nanotechnol.*, vol. 5, no. 4, pp. 314–334, Jul. 2006.

[12] G. Y. Slepyan, M. V. Shuba, S. A. Maksimenko, and A. Lakhtakia, "Theory of optical scattering by achiral carbon nanotubes and their potential as optical nanoantennas," *Phys. Rev. B, Condens. Matter*, vol. 73, p. 195416, May 2006.

[13] J. Hao and G. W. Hanson, "Electromagnetic scattering from finite-length metallic carbon nanotubes in the lower IR bands," *Phys. Rev. B, Condens. Matter*, vol. 74, p. 035119, Jul. 2006.

[14] A. I. Sotiropoulos, I.-G. V. Plegas, S. Koulouridis, and H. T. Anastassiu, "Scattering properties of carbon nanotube arrays," *IEEE Trans. Electromagn. Compat.*, vol. 54, no. 1, pp. 110–117, Feb. 2012.

[15] A. M. Hassan and E. J. Garboczi, "Electromagnetic scattering from randomly-centered parallel single-walled carbon nanotubes embedded in a dielectric slab," *IEEE Trans. Antennas Propag.*, vol. 62, no. 10, pp. 5230–5241, Oct. 2014.

[16] F. Vargas-Lara, A. M. Hassan, E. J. Garboczi, and J. F. Douglas, "Intrinsic conductivity of carbon nanotubes and graphene sheets having a realistic geometry," *J. Chem. Phys.*, vol. 143, no. 20, p. 204902, Nov. 2015.

[17] A. M. Hassan, F. Vargas-Lara, J. F. Douglas, and E. J. Garboczi, "Electromagnetic resonances of individual single-walled carbon nanotubes with realistic shapes: A characteristic modes approach," *IEEE Trans. Antennas Propag.*, vol. 64, no. 7, pp. 2743–2757, Jul. 2016.

[18] (Feb. 2016). *Nanointegris*. [Online]. Available: http://www.nanointegris.com/en/metallic

[19] (2013). *Reference Material 8281 Single-Wall Carbon Nanotubes (Dispersed, Three Length-Resolved Populations)NIST Reference Material*. [Online]. Available: https://www-s.nist.gov/srmors/view_report.cfm?srm=8281

[20] G. Y. Slepyan, M. V. Shuba, S. A. Maksimenko, C. Thomsen, and A. Lakhtakia, "Terahertz conductivity peak in composite materials containing carbon nanotubes: Theory and interpretation of experiment," *Phys. Rev. B, Condens. Matter*, vol. 81, p. 205423, May 2010.

[21] A. Buldum and J. P. Lu, "Contact resistance between carbon nanotubes," *Phys. Rev. B, Condens. Matter*, vol. 63, p. 161403, Apr. 2001.
[22] P. R. Bandaru, C. Daraio, S. Jin, and A. M. Rao, "Novel electrical switching behaviour and logic in carbon nanotube Y-junctions," *Nature Mater.*, vol. 4, no. 9, pp. 663–666, Sep. 2005.
[23] W. C. Gibson, *The Method of Moments in Electromagnetics*. Boca Raton, FL, USA: Chapman & Hall, 2008.
[24] S. A. Maier, *Plasmonics: Fundamentals and Applications*. New York, NY, USA: Springer, 2007.
[25] P. Yla-Oijala, D. C. Tzarouchis, E. Raninen, and A. Sihvola, "Characteristic mode analysis of plasmonic nanoantennas," *IEEE Trans. Antennas Propag.*, vol. 65, no. 5, pp. 2165–2172, May 2017.
[26] Y. Hadad and B. Z. Steinberg, "Electrodynamic synergy of micro-properties and macro-structure in particle arrays," in *Proc. URSI Int. Symp. Electromagn. Theory (EMTS)*, 2010, pp. 680–683.
[27] P. K. Jain, S. Eustis, and M. A. El-Sayed, "Plasmon coupling in nanorod assemblies: Optical absorption, discrete dipole approximation simulation, and exciton-coupling model," *J. Phys. Chem. B*, vol. 110, no. 37, pp. 18243–18253, Sep. 2006.
[28] S. Sheikholeslami, Y. W. Jun, P. K. Jain, and A. P. Alivisatos, "Coupling of optical resonances in a compositionally asymmetric plasmonic nanoparticle dimer," *Nano Lett.*, vol. 10, no. 7, pp. 2655–2660, Jul. 2010.
[29] D. Lee and S. Yoon, "Gold nanocube–nanosphere dimers: Preparation, plasmon coupling, and surface-enhanced Raman scattering," *J. Phys. Chem. C*, vol. 119, no. 14, pp. 7873–7882, Apr. 2015.
[30] A. M. Funston, T. J. Davis, C. Novo, and P. Mulvaney, "Coupling modes of gold trimer superstructures," *Philos. Trans. R. Soc. Math. Phys. Eng. Sci.*, vol. 369, no. 1950, pp. 3472–3482, Sep. 2011.
[31] L. Chuntonov and G. Haran, "Trimeric plasmonic molecules: The role of symmetry," *Nano Lett.*, vol. 11, no. 6, pp. 2440–2445, Jun. 2011.
[32] D. E. Gómez, Z. Q. Teo, M. Altissimo, T. J. Davis, S. Earl, and A. Roberts, "The dark side of plasmonics," *Nano Lett.*, vol. 13, no. 8, pp. 3722–3728, Aug. 2013.
[33] A. I. Dolinnyi, "Nanometric rulers based on plasmon coupling in pairs of gold nanoparticles," *J. Phys. Chem. C*, vol. 119, no. 9, pp. 4990–5001, Mar. 2015.
[34] J. A. Bordley, N. Hooshmand, and M. A. El-Sayed, "The coupling between gold or silver nanocubes in their homo-dimers: A new coupling mechanism at short separation distances," *Nano Lett.*, vol. 15, no. 5, pp. 3391–3397, May 2015.
[35] S. A. Tretyakov, F. Mariotte, C. R. Simovski, T. G. Kharina, and J. P. Heliot, "Analytical antenna model for chiral scatterers: Comparison with numerical and experimental data," *IEEE Trans. Antennas Propag.*, vol. 44, no. 7, pp. 1006–1014, Jul. 1996.
[36] J. C.-E. Sten and D. Sjoberg, "Low-frequency scattering analysis and homogenisation of split-ring elements," *Prog. Electromagn. Res. B*, vol. 35, pp. 187–212, 2011.
[37] F. Mariotte, S. A. Tretyakov, and B. Sauviac, "Isotropic chiral composite modeling: Comparison between analytical, numerical, and experimental results," *Microw. Opt. Technol. Lett.*, vol. 7, no. 18, pp. 861–864, 1994.
[38] A. Ishimaru, S.-W. Lee, Y. Kuga, and V. Jandhyala, "Generalized constitutive relations for metamaterials based on the quasi-static Lorentz theory," *IEEE Trans. Antennas Propag.*, vol. 51, no. 10, pp. 2550–2557, Oct. 2003.
[39] V. S. Asadchy, I. A. Faniayeu, Y. Ra'di, and S. A. Tretyakov, "Determining polarizability tensors for an arbitrary small electromagnetic scatterer," *Photon. Nanostruct.-Fundam. Appl.*, vol. 12, no. 4, pp. 298–304, Aug. 2014.
[40] J. D. Jackson, *Classical Electrodynamics*, 3rd ed. New York, NY, USA: Wiley, 1999.
[41] J. F. Douglas and E. J. Garboczi, "Intrinsic viscosity and the polarizability of particles having a wide range of shapes," in *Advances in Chemical Physics*, vol. 91, I. Prigogine and S. A. Rice, Eds. Hoboken, NJ, USA: Wiley, 1995, pp. 85–153.
[42] D. J. Audus, A. M. Hassan, E. J. Garboczi, and J. F. Douglas, "Interplay of particle shape and suspension properties: A study of cube-like particles," *Soft Matter*, vol. 11, pp. 3360–3366, 2015.
[43] T. Aste and D. L. Weaire, *The Pursuit of Perfect Packing*, 2nd ed. New York, NY, USA: Taylor & Francis, 2008.
[44] S. Torquato, *Random Heterogeneous Materials: Microstructure and Macroscopic Properties*. New York, NY, USA: Springer, 2002.
[45] A. Lakhtakia, G. Ya. Slepyan, S. A. Maksimenko, A. V. Gusakov, and O. M. Yevtushenko, "Effective medium theory of the microwave and the infrared properties of composites with carbon nanotube inclusions," *Carbon*, vol. 36, no. 12, pp. 1833–1839, 1998.
[46] R. Takahata, S. Yamazoe, K. Koyasu, and T. Tsukuda, "Surface plasmon resonance in gold ultrathin nanorods and nanowires," *J. Amer. Chem. Soc.*, vol. 136, no. 24, pp. 8489–8491, Jun. 2014.
[47] M. V. Shuba *et al.*, "Experimental evidence of localized plasmon resonance in composite materials containing single-wall carbon nanotubes," *Phys. Rev. B, Condens. Matter*, vol. 85, p. 165435, Apr. 2012.
[48] M. V. Shuba, A. V. Melnikov, A. G. Paddubskaya, P. P. Kuzhir, S. A. Maksimenko, and C. Thomsen, "Role of finite-size effects in the microwave and subterahertz electromagnetic response of a multiwall carbon-nanotube-based composite: Theory and interpretation of experiments," *Phys. Rev. B, Condens. Matter*, vol. 88, p. 045436, Jul. 2013.
[49] Q. Zhang *et al.*, "Plasmonic nature of the terahertz conductivity peak in single-wall carbon nanotubes," *Nano Lett.*, vol. 13, no. 12, pp. 5991–5996, Dec. 2013.
[50] A. A. Kishk, X. Zhang, A. W. Glisson, and D. Kajfez, "Numerical analysis of stacked dielectric resonator antennas excited by a coaxial probe for wideband applications," *IEEE Trans. Antennas Propag.*, vol. 51, no. 8, pp. 1996–2006, Aug. 2003.
[51] A. Sangiovanni, J. Y. Dauvignac, and Ch. Pichot, "Stacked dielectric resonator antenna for multifrequency operation," *Microw. Opt. Technol. Lett.*, vol. 18, no. 4, pp. 303–306, Jul. 1998.

Ahmed M. Hassan (S'07–M'12) received the B.Sc. (with highest Hons.) and M.Sc. degrees in electronics and communications engineering from Cairo University, Giza, Egypt, in 2004 and 2006, respectively, and the Ph.D. degree in electrical engineering from the University of Arkansas, Fayetteville, AR, USA, in 2010.

From 2011 to 2012, he was a Post-Doctoral Researcher with the Department of Electrical Engineering, University of Arkansas. From 2012 to 2015, he was a Post-Doctoral Researcher at the National Institute of Standards and Technology, Gaithersburg, MD, USA. He is currently an Assistant Professor with the Computer Science Electrical Engineering Department, University of Missouri-Kansas City, Kansas City, MO, USA. His current research interests include nanoelectromagnetics, bioelectromagnetics, nondestructive evaluation, and experimental microwave and terahertz imaging.

Dr. Hassan was a recipient of the Doctoral Academy Fellowship at the University of Arkansas and the Outstanding Poster Award in the 2014 21st Annual NIST Sigma Xi Post-Doctoral Poster Presentation.

Fernando Vargas-Lara received the B.S. degree in physics from the National Polytechnic School, Quito, Ecuador, in 2003, and the Ph.D. degree in physics from Wesleyan University, Middletown, CT, USA, in 2013.

Since 2013, he has been a Post-Doctoral Researcher with the Materials Science and Engineering Division, National Institute of Standards and Technology (NIST), Gaithersburg, MD, USA. His current research interests include the study of the self-assembly of DNA-based structures, the transport and structural properties of polymers and complex shaped particles, and the electromagnetic properties of carbon nanotube and graphene composites.

Dr. Vargas-Lara is a member of the American Physics Society and the American Chemistry Society. He received the Material Measurement Laboratory Distinguished Associate Award, NIST, in 2015, and the Soft Matter Poster Prize at the Boulder Summer School: Polymers in Soft and Biological Matter, University of Colorado Boulder, Boulder, CO, USA, in 2012.

Jack F. Douglas received the B.Sc. degree in chemistry and the M.S. degree in mathematics from Virginia Commonwealth University, Richmond, VA, USA, in 1979 and 1981, respectively, and the Ph.D. degree in chemistry from the University of Chicago, Chicago, IL, USA, in 1986, under the direction of Prof. K. Freed.

He was an IBM Graduate Fellow, from 1985 to 1986. He was the first NATO Fellow at the Cavendish Laboratory, Cambridge, U.K., where he was under the direction of Prof. S. Edwards. He was a National Research Council Post-Doctoral Fellow at the National Institute of Standards and Technology (NIST), Gaithersburg, MD, USA, and then became a Research Scientist in the Polymers Division until he was promoted to the position of NIST Fellow, the most senior scientific position at NIST. He has authored over 400 papers covering a broad range of topics in statistical physics such as transport properties of suspensions, percolation theory, random and self-avoiding walks, random surfaces, protein dynamics, the physics of worm-like polymers such as DNA, phase separation in polymer blends and solutions, self-assembly of block copolymers, polymer nanocomposites, rubber elasticity, self-assembly and molecular binding, crystallization under far from equilibrium conditions, the dynamics of grain boundaries, the dynamics of nanoparticles and thin films, photopolymerization, renormalization group theory, path-integration, and fractional calculus, surface interacting polymers, dewetting of polymer films, supercooled liquids and glasses, and entanglement interactions in polymer fluids.

Dr. Douglas was an APS Fellow, Bronze Medal—Department of Commerce, five-year rotation as an Editorial Board Member of *Physical Review Letters*, and he was selected for Phi Kappa Phi and Sigma Xi, and for the American Chemical Society Senior Award at VCU.

Edward J. Garboczi received the B.S. (with highest Hons.) degree in physics and the Ph.D. degree in condensed matter physics (theory) from Michigan State University, East Lansing, MI, USA, in 1980 and 1985, respectively.

From 1985 to 1988, he was a Research Physicist with the Armstrong World Industries, Inc., Lancaster, PA, USA. From 1988 to 2014, he was a Physicist, a Group Leader, and finally a Fellow in the Materials and Structural Systems Division, National Institute of Standards and Technology (NIST), Gaithersburg, MD, USA. In 2014, he joined the Division of Applied Chemicals and Materials, NIST, Boulder, CO, USA. His current research interests include computational materials science, porous materials, electrical properties of nanocomposites, and 3-D particle shape analysis of a wide range of particles including gravel, sand, cement, chemical explosives, lunar soil, and metal powder for additive manufacturing.

Dr. Garboczi is a Fellow of the American Concrete Institute, the American Ceramic Society. He was a recipient of the ACI Robert E. Philleo Award, the ACerS Della Roy Lecture Award, the ACerS Edward C. Henry Best Paper Award (Electronics Division), and a Silver Medal from the Department of Commerce for the creation of the Virtual Cement and Concrete Testing Laboratory.